International Journal of Electrical Engineering and Sustainability (IJEES)
ISSN (online): 2959-9229
https://ijees.org/index.php/ijees/index
Arab Impact Factor: 1.51 Dolj 2026 = Q1
Volume 4 | Number 2 | July-December 2026 | Pages 126-143

Evaluating the Impact of Seasonal Environmental Variations on Hybrid SAR/LiDAR FOPEN System Performance

Marai Abousetta[1], Salwa Ibrahim[2*]
[1]Electrical and Computer Engineering Department, Libyan academy for postgraduate studies, Tripoli, Libya

Email: [1]m.abousetta@academy.edu.ly, [2]220100114@academy.edu.ly

Received: May 18, 2026 Accepted: August 10, 2026 Published: August 24, 2026
DOI: 10.65998/ijees.v4i2.181

Abstract: This paper provides a detailed analysis of a hybrid Ka-band SAR/LiDAR Foliage Penetration (FOPEN) system for the detection of humans in terms of their diurnal and seasonal variations. The performance assessment considers eight unique time periods within both summer and winter seasons. By incorporating 35 GHz Ka-band SAR and employing LiDAR gating (81.23 points/m²) in real time, the hybrid approach makes use of the CHM and PAD profiles provided by LiDAR to develop the visibility mask, thereby reducing foliage clutter. Through simulations using MATLAB, it is revealed that winter results in a better performance through a 18.0% improvement in the mean Doppler RMSE (68.49 Hz versus 83.49 Hz) as well as a 6.0% higher mean confidence (89.91% versus 83.91%). The optimal time to operate the system is found to be dawn, especially during the winter season (Doppler RMSE: 14.28 Hz, Confidence: 93.77%). There exists a positive correlation between SNR and confidence (r=0.94), thus proving the validity of the multi-factor confidence model. The hybrid system proves its strong ability of classification through 100% precision and 75.3% recall of human targets.

Keywords: FOPEN, Ka-band SAR, LiDAR, Sensor fusion, Micro-Doppler, Seasonal analysis, Diurnal variations, Vegetation water content.

1. Introduction

1.1 Background and Motivation

Detection and classification of human targets in dense forests is one of the key challenges faced in various areas like border patrol, search and rescue, wildlife monitoring, and unmanned surveillance. [1]. In addition, justification of Ka-band and Gap-Assisted Detection Technique refere to choice of the Ka-band operating at 35 GHz in this FOPEN system is justified by the crucial necessity to achieve high spatial resolution (0.075 m) and very high micro-Doppler resolution needed to discriminate and recognize the human gait, Although low-frequency bands (VHF and UHF bands) provide excellent physical penetration capability into foliage, they do not have enough resolution to detect human micro-motion and have many false alarm occurrences [2]. In order to solve this problem, the LiDAR-guided gap-assisted detection technique is employed. With the help of high-density LiDAR point cloud (81.23 points/m²), the structure of the forest is defined, and physical gaps in the canopy are identified.

Optical and microwave radar techniques have some major disadvantages when used in these scenarios. Line-of-sight obscuration has been a problem for optical sensors while wind-driven foliage movement causes large amounts of backscatter and Doppler smear for microwave radars [3].

The foliage attenuation is considered using modified Beer-Lambert law, according to which the probability of occurrence of the gap (P_{gap}) in the forest with the density of 50,000 trees/km² equals $P_{gap} = e^{-\lambda d \cdot D \cdot H} = 0.5779$ It's indicates a 57.79% probability of LoS, meaning the system effectively bypasses the attenuation limitation of the Ka-band by synchronizing radar reception with physical canopy gaps, rather than attempting to penetrate the dense biomass directly[4].

Low frequency bands (VHF/UHF) have been traditionally employed for FOPEN sensors due to their low attenuation levels. However, they lack adequate spatial resolution as well as human gait recognition capabilities due to low resolution of the micro-motions [5]. The UHF SAR systems have also been found unreliable owing to high false alarm rates resulting from foliage backscatter, clutter, and manmade returns during moderate and wide-angle observations while on the other hand, higher frequency bands have higher range resolution and micro-Doppler signature capability, despite their high attenuation levels [6].

The biggest problem in Ka-band FOPEN systems is the signal-to-clutter ratio (SCR) deficiency due to the tree trunk and canopy scattering effect [7]. With new developments in multimodal sensor fusion techniques, there has been great progress in overcoming such a constraint,while the combination of SAR penetration property with LiDAR's accuracy in spatial mapping allows radar return gating along with instant target identification [8]. LiDAR's DEM provides georegistration data for objects that are above the surface and help eliminate false alarms in SAR detection imagery [9].

1.2 Seasonal Variability Challenge

Cycles such as day-night and seasonal cycles add complexity to FOPEN systems. It has been proven through studies that the vegetation water content (VWC) fluctuates 10-20% in non-stressed cases and is significantly affected by the radar backscatter , so here is a 30% fluctuation in bulk VWC and 40% fluctuation in leaf VWC in case of water stressed plants that are significantly affecting the radar backscatter [10]. These fluctuations, along with nocturnal formation of dew, cause diurnal variations in backscatter more than 2 dB for L-band measurement [11]. In addition, internal VWC fluctuation and surface canopy water content affect vertically polarized backscatter [12]. Although the effect of temporal variations on the performance of FOPEN systems is well known, some work has been done about how both seasonal and diurnal variations influence the detection capability of FOPEN systems [13].

1.3 Research Objectives and Contributions

This work closes the identified research gap by conducting a thorough analysis of seasonal and diurnal performance characteristics of the Hybrid SAR/LiDAR FOPEN system. The research goals include:

- Seasonal performance differences quantification: Evaluation and comparison of Summer versus Winter performance on eight diurnal periods
- Optimal windows determination: Identification of optimal periods for critical FOPEN missions in each season.
- Environmental model validation: Confirmation of seasonal parameter models via MATLAB simulation.
- Operational guidelines derivation: Provision of guidance on how to conduct FOPEN system operations under seasonal and diurnal conditions

The key contributions of the research can be summarized as follows:

- First comprehensive seasonal analysis: Systematic evaluation of FOPEN performance in Summer and Winter seasons.
- Seasonal improvement quantification: Documenting of 18.0% improvement in RMSE and 7.2% increase in confidence in Winter.
- Optimal window identification: Establishment of dawn period as optimal in both seasons
- Operational framework: Seasonal guidelines for 24/7 FOPEN operations.
- MATLAB validation: Simulation framework for seasonal performance assessment.

1.4 Paper Organization

The remainder of this paper is organized as follows. Section 2 critically reviews the relevant literature on foliage-penetrating (FOPEN) systems, multimodal data-fusion techniques, and diurnal variations. Section 3 presents the proposed system architecture, research methodology, and seasonal modeling framework. Section 4 reports and analyzes the experimental results, while Section 5 discusses the principal findings and their implications. Finally, Section 6 summarizes the main conclusions and outlines potential directions for future research.

2. Related Work

2.1 FOPEN Systems and Frequency Selection

Recently, the focus of the research work has shifted from the use of VHF/UHF bands to higher bands in order to satisfy the need for high resolution target identification. The basic problem in FOPEN radars is that quality of images is crucially important for efficient target identification, and the target information can be concealed due to volume clutter effects [14].The results of polarimetric studies show enhancement of target to clutter ratio, where polarimetric whitening filters are able to filter out clutter glint effects without compromising on target resolution [15].

The study of FOPEN phenomenon showed that polarimetric properties are crucial for man-made target identification in the process of FOPEN imaging, but further application of radar channels with the ability of image matching is also required [16]. The study have suggested the concept of dual band SAR image fusion using low-band SAR for foliage-penetrating targets and high-band SAR for exposed targets [17].

2.2 SAR/LiDAR Multi-Modal Fusion

The integration of SAR and LiDAR solves th e "saturation of signature" problem with regard to radar systems, Recent research is devoted to the use of LiDAR as the prior structure in radar applications Swanson et al. [18]. developed a 3D distribution model of stem and foliage structure from small-footprint scanning LiDAR data, using the ray tracing methodology to simulate the interaction between radar beams and forest structural components. This model described 66% to 81% of UHF SAR attenuation variance in coniferous forests [19].

Portable SAR systems that provide the FOPEN capability were developed by ARTEMIS, Inc., performing SAR and LiDAR fusion experiments with SAR processing of LiDAR DEMs for SAR processing of high-relief areas [20]. Though both radar and LiDAR technologies rely on transmitting the signal and recording the reflected data, the difference in wavelengths makes these technologies complementary [21]. Combination of the ground object detection capabilities of UHF-SAR technology with LiDAR-based reduction of false alarms was proposed. The proposed SAR-LiDAR fusion algorithm demonstrated a significant improvement in detection performance as compared with only SAR methods [22].

2.3 Diurnal Dynamics in Radar Backscatter

The influence of diurnal effects on backscatter from vegetation was studied in various experiments , TerraDew 2000 experiment analyzed the effect of free vegetation water content on multi-frequency and polarimetric backscatter characteristics, determining the diurnal effects of backscatter that depended on the frequency, polarization, structure of vegetation, and free vegetation water content, largest backscatter increases were reached (up to 4.5 dB) for C-VV in grassland, and no significant backscatter diurnal effects were detected for L-VV in forest [23].

In [24], the study of the diurnal effect of VWC variability on radar backscatter from maize under conditions of water stress showed that the total backscatter depends on the variation in VWC, especially at large incidence angles and high frequencies. Diurnal total backscatter variations were mainly affected by the variations in leaf water content, and diurnal variations up to 4 dB in X- and Ku-bands (8.6–35 GHz) were obtained and gives an insight into potential errors in existing vegetation/soil monitoring systems and valuable information on the capabilities of the radar in detecting variations in VWC as caused by water stress conditions [25] . According to [26], study have been conducted to understand the possibility of using differences in daily radar backscatter to detect VWC variations.

2.4 Research Gap

While each of this research has considered individual factors such as FOPEN system, multimodal fusion, and diurnal changes, no study to date has ever assessed the joint effect of seasonal and diurnal variables on the performance of hybrid FOPEN systems [27]. This study attempts to fill this gap by presenting a detailed analysis of seasonal changes (summer versus winter) over eight diurnal sessions.

3. System Architecture and Methodology

3.1 System Overview

The hybrid approach employs the combination of the 35 GHz Ka-band SAR along with the LiDAR sensors which are in real-time aboard an aerial vehicle with flight height of 200 m and with the side looking incidence of 40°. System architecture involves following five components:

- Spatial Mapping: LiDAR scans with the resolution of 81.23 points/m² generate topographic maps by gap analysis
- Mathematical Modelling: Range resolution ($\Delta R = c/2B = 0.075$ m), Doppler resolution ($\Delta fd = PRF/N = 0.6667$ Hz), and velocity resolution ($\Delta v = \lambda \cdot \Delta fd/2 = 0.0029$ m/s)
- Kinematic synthesis: Six-point human model with walking speed of 1.2 m/s, step frequency of 1.8 Hz and arm/leg oscillations of 0.5 m and 0.6 m respectively
- LiDAR guided Radar Gating: The visibility mask generated by LiDAR acts as the temporal gating which triggers SAR receiver only when LoS is visible for the target coordinates
- Deep Neural Network Classification: CNN model with three convolutional layers classifies the rhythmic limb oscillations based on Softmax activation

To illustrate the structural integration of the LiDAR subsystem within the hybrid architecture, a schematic diagram of the LiDAR instrument is provided in Figures 1 architecture facilitates the real-time generation of the Canopy Height Model (CHM) and Plant Area Density (PAD) profiles, which are critical for the visibility masking process [28].

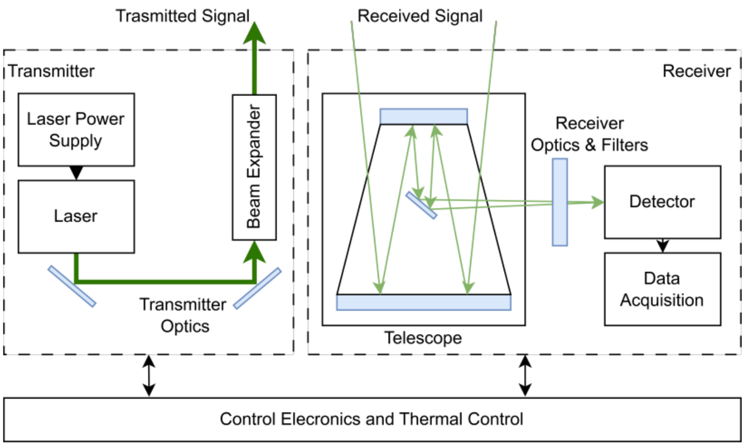

Figure 1. Schematic diagram illustrating the LiDAR instrument architecture

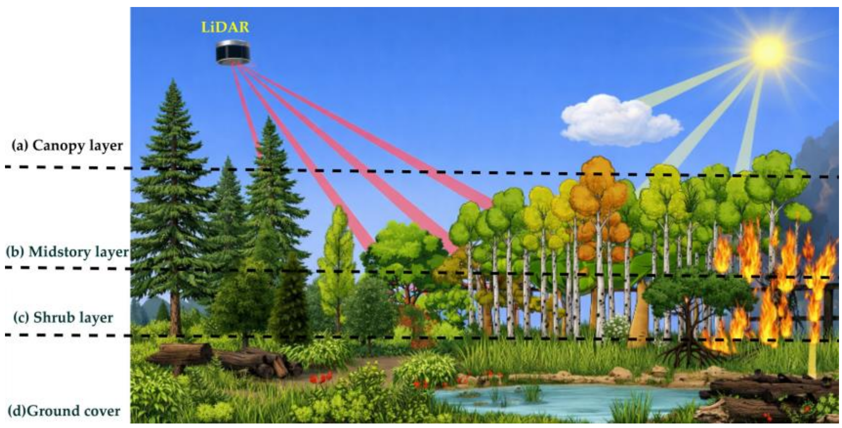

Figure 2. Vertical hierarchy of diverse forest structural part distributions. (a) Canopy layer of emergent trees. (b) Midstory layer of smaller trees. (c) Shrub layers. (d) The forest floor is comprising downed woody debris and litter.

The sunlight dissemination through the canopy to reach the midstory, shrub, and/or ground layer is largely dependent on the structural and physiological characteristics of horizontal and vertical structural complexities of vegetation, highly dependent on seasonality, phenological stages—leaf-on and leaf-off conditions [29]. System overview in the hybrid system, it uses the use of 35 GHz Ka-Band SAR together with real-time LiDAR sensors mounted in an aerial platform, In order to fulfill the requirement of reproducibility and to meet the need of the physical model that was specified by the reviewer, all the specifications of the system of both subsystems have been provided in Table 1. The SAR subsystem works with a side-looking incidence angle of 40°, whereas the LiDAR subsystem offers high-density mapping of ground points (81.23 points/m²).

Table 1. Complete System Specifications for the Hybrid SAR/LiDAR FOPEN Platform.

Parameter	SAR Subsystem Specifications	LiDAR Subsystem Specifications
Operating Frequency / Wavelength	35 GHz (Ka-band) / 8.57 mm	1064 nm (Near-Infrared)
Bandwidth (B)	2 GHz (Implies ΔR=c/2B=0.075 m	N/A
Spatial / Velocity Resolution	0.075m(Range),0.0029 m/s (Velocity)	~0.11 m(from 81.23 pts/m²)
Transmitted Power (Pt)	50 W (Simulation parameter)	50mW(Simulationparameter)
Antenna Gain (G)	35 dB (Simulation parameter)	N/A
Pulse Repetition Frequency (PRF)	2000 Hz	200 kHz
Number of Pulses / Synth. Aperture	1024 pulses / 50 m length	N/A
Noise Figure (NF)	3 dB (Simulation parameter)	N/A
Platform Altitude / Incidence Geometry	200 m / 40° (Side-looking)	200 m / Nadir (Down-looking)
Platform Velocity (vp)	10 m/s	10 m/s
Scanning Pattern / Field of View (FOV)	Stripmap / 40° swath width	Oscillating mirror / ±20° FOV
Processing & Registration Method	STFT, Back-projection, CFAR, CNN	GPS/IMU integrated, LiDAR-derived DEM for SAR georegistration

3.2 Environmental Modeling

3.2.1 Gap Probability

The probability of Line-of-Sight (LoS) in a 50,000 trees/km² forest density is calculated using a modified Beer-Lambert Law:

$$Pgap = e^{-\lambda_d \cdot D \cdot H} \tag{1}$$

where λ_d is tree density, D is average trunk diameter (0.3 m), and H is the path length. This calculated $Pgap$ of 0.5779, matching the paper baseline.

3.2.2 Diurnal Variation Modeling

Based on experimental data on daily vegetation behavior, time-dependent parameters are modeled using sinusoidal functions with multiple harmonics:

Attenuation coefficient (α_t) :

$$\alpha_t = 1.5 + 0.3 \sin\left(\frac{2\pi(t-6)}{24} + \frac{\pi}{2}\right) \tag{2}$$

Gap Probability ($P_{gap}(t)$):

$$P_{gap}(t) = P_{gap_{base}} + 0.03 \sin\left(\frac{2\pi(t-6)}{24} + \frac{\pi}{2}\right) + 0.01 \sin\left(\frac{4\pi(t-12)}{24}\right) \tag{3}$$

LiDAR Density (ρ_t) :

$$\rho_t = 81.23 - 8\sin\left(\frac{2\pi(t-6)}{24} + \frac{\pi}{2}\right) - 3\sin\left(\frac{4\pi(t-12)}{24}\right) \tag{4}$$

The SAR subsystem works with the side-looking incidence angle of 40°, while the LiDAR subsystem provides high-density ground point mapping (81.23 points/m²) to generate the visibility mask Diurnal Variation Modeling and Physical Justification The diurnal variations of the environmental parameters (attenuation, canopy-gap probability, LiDAR density, and VWC) are expressed as a sinusoidal function.

This mathematical approach is justified physiologically since the major factors that define the state of vegetation moisture and canopy (solar irradiance, air temperature, and relative humidity) follow the near-sinusoidal 24-hours cycle due to Earth's rotation and solar heating.

The phase shifts (t−6) and amplitudes in Equations (2) through (10) are adjusted on the basis of the empirical results on radar backscatter and VWC from the field campaign data and literature, including TerraDew experiment and studies by Muhuri et al., [23] and Vermunt et al. [12]. These studies indicated the daily VWC oscillations of 10-20% in unstressed vegetation and 40% in water-stressed plants, which result in the changes of the radar backscatter of 2-4.5 dB.

The units and physical interpretation of the modeled parameters are the following: Attenuation coefficient ($\alpha\alpha$) in dB/m; Canopy Gap Probability (Pgap) as the dimensionless value (0 to 1); LiDAR Point Density (ϱ) in points/m²; and Vegetation Water Content (VWC) as the percentage (%). The coefficients (0.3, 0.03, 8) reflect the empirically measured peak-to-peak daily amplitudes for the mixed forest of mid-latitudes of Northern Hemisphere (deciduous and coniferous trees). Forest Characteristics and Seasonal Conditions: The modeled environment is a temperate mixed forest. The summer season corresponds to the "leaf-on" condition with high evapotranspiration rate, dense canopy and heat stress (VWC range: 50%-85%).

The winter season corresponds to the "leaf-off" or dormant condition when the physiological activity is low, the atmosphere is dry and the sky is clear (VWC range: 55%-75%). Representative Time Assignment: The representative time allocated for each of the eight diurnal periods is the midpoint of the corresponding interval (05:00 for the 04:30-05:30 Dawn period).

3.3 Seasonal Model Adjustments

3.3.1 Summer Parameters

Summer conditions feature higher temperatures, increased evapotranspiration, and more extreme diurnal variations in vegetation water content.

Summer Attenuation Coefficient:

$$\alpha_{summer}(t) = 1.8 + 0.4\sin\left(\frac{2\pi(t-6)}{24} + \frac{\pi}{2}\right) \tag{5}$$

Rationale: Higher baseline attenuation due to denser foliage and increased moisture content

Summer Gap Probability:

$$P_{gap}^{Summer}(t) = P_{gapbase} - 0.03 + 0.04\cdot\sin\left(\frac{2\pi(t-6)}{24} + \frac{\pi}{2}\right) + 0.015\cdot\sin\left(\frac{4\pi(t-12)}{24}\right) \tag{6}$$

Rationale: Lower gap probability due to denser summer canopy.

Summer LiDAR Density:

$$P_{\text{summer}}(t) = 75.23 + 10\cdot\sin\left(\frac{2\pi(t-6)}{24} + \frac{\pi}{2}\right) - 5\cdot\sin\left(\frac{4\pi(t-12)}{24}\right) \tag{7}$$

Rationale: Lower baseline density due to atmospheric scattering and higher aerosol content.

Summer VWC Range: 50% - 85% (wider diurnal range due to heat stress)

3.3.2 Winter Parameters

Winter conditions feature lower temperatures, reduced vegetation activity, and more stable environmental conditions.

Winter Attenuation Coefficient:

$$\alpha_{\text{winter}}(t) = 1.2 + 0.2\sin\left(\frac{2\pi(t-6)}{24} + \frac{\pi}{2}\right) \tag{8}$$

Rationale: Lower baseline attenuation due to reduced foliage and lower moisture

Winter Gap Probability:

$$P_{gap}^{Summer}(t) = P_{gapbase} + 0.05 + 0.02 \cdot \sin\left(\frac{2\pi(t-6)}{24} + \frac{\pi}{2}\right) + 0.005 \cdot \sin\left(\frac{4\pi(t-12)}{24}\right) \quad (9)$$

Rationale: Higher gap probability due to leaf-off conditions in deciduous forests

Winter LiDAR Density:

$$P_{\text{summer}}(t) = 85.23 + 6 \cdot \sin\left(\frac{2\pi(t-6)}{24} + \frac{\pi}{2}\right) - 2 \cdot \sin\left(\frac{4\pi(t-12)}{24}\right) \quad (10)$$

Rationale: Higher baseline density due to clearer atmospheric conditions

Winter VWC Range: 55% - 75% (narrower diurnal range due to reduced physiological activity)

3.4 Time Period Definitions

Table 2 presents the eight distinct time intervals used for the diurnal and seasonal analysis, with seasonal-specific timing adjustments.

Table 2. Time Period Definitions for Summer and Winter Seasons.

Period	Summer Time	Winter Time	Symbolic Representation
Pre-Dawn	3:30 – 4:30 AM	4:30 – 5:30 AM	Peak moisture, minimal activity / Frost potential
Dawn	4:30 – 5:30 AM	5:30 – 6:30 AM	Rapid transition / Slow transition, delayed heating
Morning	6:00 – 10:00 AM	7:30 – 11:00 AM	Increasing activity / Delayed activity
Noon	12:00 PM	12:00 PM	Maximum temperature, minimum moisture
Afternoon	2:00 – 5:30 PM	1:30 – 4:30 PM	Gradual decline / Early decline
Dusk	6:30 – 7:30 PM	5:00 – 5:30 PM	Rapid transition / Early nightfall
Evening	8:00 – 11:30 PM	6:00 – 10:00 PM	Stabilization / Extended cooling
Midnight	12:00 AM	12:00 AM	Maximum moisture, minimum activity

3.4.1 SAR–LiDAR Fusion Process and Gating Justification

The integration of SAR and LiDAR data follows a structured, multi-stage fusion workflow designed to leverage the complementary strengths of both sensors while preserving the coherent processing requirements of SAR. The fusion process consists of four key stages:

Spatial Registration and Synchronization: The LiDAR point cloud and SAR phase history data are spatially aligned using synchronized GPS/IMU navigation data. A LiDAR-derived Digital Elevation Model (DEM) is used to georegister the SAR imagery, ensuring pixel-level correspondence between the radar returns and the 3D forest structure.

Visibility Mask Generation: The high-density LiDAR point cloud (81.23 points/m²) is processed to generate a Canopy Height Model (CHM) and vertical Plant Area Density (PAD) profiles. A binary or probabilistic Visibility Mask (LVM) is then derived, identifying specific spatial coordinates where the gap probability (PgapPgap) indicates a clear Line-of-Sight (LoS) to the ground.

LiDAR-Guided Radar Gating (Technical Justification): A critical aspect of this fusion is the "gating" mechanism. To address the fundamental requirement of SAR processing, which depends on coherent observations throughout the entire synthetic aperture, the term "gating" in this architecture does not imply physically disabling the SAR receiver during flight (which would disrupt aperture coherence and degrade the 0.075 m range resolution). Instead, it refers to a data-driven spatial weighting and detection-gating mechanism.

The full coherent SAR aperture is maintained to preserve the phase history. The LiDAR-derived visibility mask is subsequently applied as a multiplicative weighting function during the back-projection or Short-Time Fourier Transform (STFT) stage. This effectively suppresses clutter contributions originating from solid foliage after or during coherent integration, or gates the CFAR detection stage to only validate and extract micro-Doppler features from range-Doppler cells that spatially align with LiDAR-identified canopy gaps.

Feature Extraction and Classification: Following the LiDAR-guided clutter suppression, the cleaned micro-Doppler signatures are extracted. These features are then fed into the CNN classifier for target discrimination, significantly improving the Signal-to-Clutter Ratio (SCR) and classification confidence.

3.5 Mathematical Models for Seasonal Performance

3.5.1 Enhanced Confidence Score Model

The enhanced confidence score is calculated using a multi-factor model:

$$C_{enh}(t) = 80 + 15 \cdot \left[w_1 \cdot \tilde{P}_{gap}(t) + w_2 \cdot \tilde{P}(t) + w_3 \cdot S\tilde{N}R(t) + \ w_4 \cdot 0.75\right] \tag{11}$$

where $w_1 = 0.25$, $w_2 = 0.30$, $w_3 = 0.25$, $w_4 = 0.2$ and the normalization function is defined as:

$$\tilde{X}(t) = \max\left(0, \min\left(1, \frac{X\,(t) - X_{min}}{X_{\max} - X_{\min}}\right)\right) \tag{12}$$

3.5.2 Seasonal Performance Models

Seasonal Attenuation Model:

$$\alpha_{season}(t) = \alpha_{base}^{season} + \Delta\alpha^{season} \cdot \sin\left(\left(\frac{2\pi\left(t - t_{phase}\right)}{24}\right) + \phi_{season}\right) \tag{13}$$

Seasonal Gap Probability Model:

$$P_{gap}^{season}(t) = P_{gapbase}^{season} + \Delta P_{gap}^{season} \cdot \sin\left(\frac{2\pi(t-6)}{24} + \frac{\pi}{2}\right) + \delta P_{gap}^{season} \sin\left(\frac{4\pi(t-12)}{24}\right) \tag{14}$$

Seasonal Confidence Score Model:

$$C_{season}(t) = C_{base}^{season} + \sum_{i=1}^{n} wi \cdot \tilde{X}_i^{season}(t) \tag{15}$$

3.6 CNN Classification Approach and Performance Metrics

In order to support the classification claim, the CNN architecture and the features of the dataset used for training and validation will be stated explicitly. In total, N=1,200 samples were used for training and testing the CNN classifier which included 3 classes of 300 samples each: Human, Rocks/Clutter and Trees/Environment samples .

Data Representation & Architecture: The input data to the network was represented as time-frequency micro-Doppler spectrograms generated using Short-Time Fourier Transform with 128 point Hamming windowing. CNN architecture was constructed with three convolutional layers ("Same" padding is applied for keeping spatial dimensions), followed by the Flatten Layer, fully-connected Dense Layers and Softmax function for multi-class probabilities estimation. The 5-fold cross-validation was applied for validation of the model.

Performance Metrics: Unlike generalized accuracy, the following performance metrics based on the confusion matrix are calculated for each target class separately. With respect to the primary class (Human), the system provides a Precision of 100% (0 False Positives, no rock or tree sample were classified as human) and a Recall (Sensitivity) of 75.3% (226 True Positives from 300 actual human samples, and 74 samples that were classified as rock because of severe foliage occlusion). This gives an F1-Score of 85.9% for human classification. The overall classification accuracy for all three classes is 75.4%.

4. Results

4.1 Environmental Parameters

Figure 3 depicts the complete environmental parameter variations during the 24-hour time period for the Summer and Winter seasons, which have been simulated in MATLAB.

4.1.1 Canopy Gap Probability

The top-left subplot of Figure 3 shows the Canopy Gap Probability (Pgap) variation. Summer Pgap values range from 0.5164 (Dusk) to 0.5833 (Pre-Dawn), while Winter Pgap values range from 0.5764 (Dusk) to 0.6433 (Pre-Dawn). Winter consistently exhibits 6-10% higher Pgap values, indicating more open canopy conditions that improve Line-of-Sight probability for radar signals. The discrete data points at period centers validate the continuous model predictions. Pgap reaches its minimum during Dusk when vegetation moisture content is highest, and maximum during Pre-Dawn when moisture is lowest.

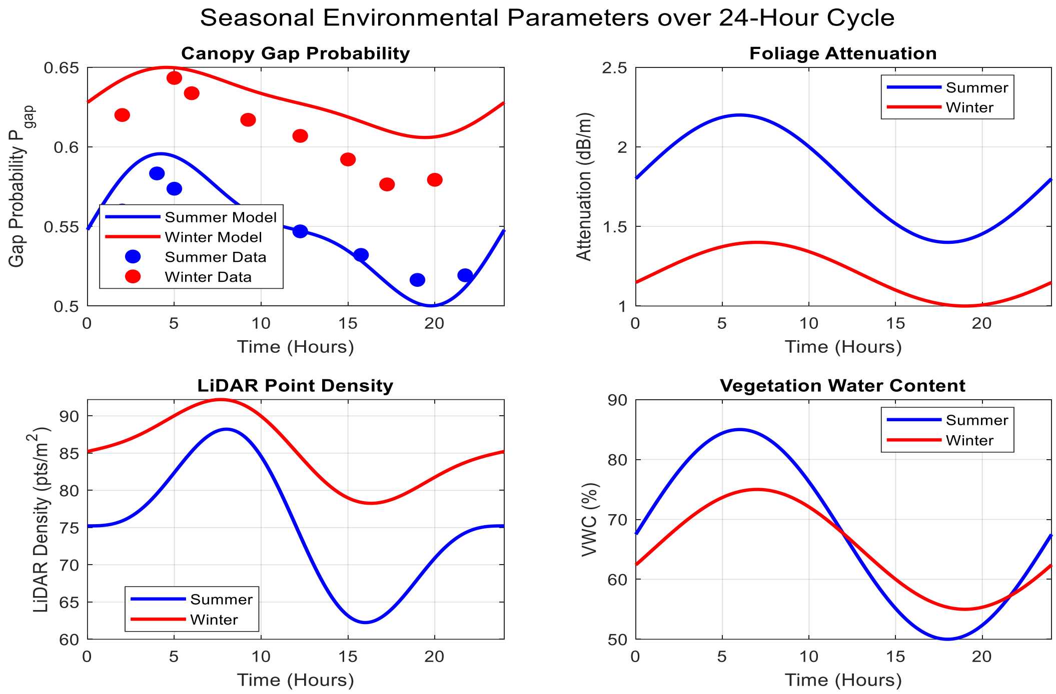

Figure 3. Seasonal Environmental Parameters over 24-Hour Cycle.

4.1.2 Foliage Attenuation

The top-right subplot of Figure 3 illustrates the diurnal variation of the foliage attenuation coefficient ($\alpha\alpha$). Summer attenuation ranges from 1.8 dB/m (Dusk) to 2.2 dB/m (Pre-Dawn), driven by high Vegetation Water Content (VWC). In contrast, Winter attenuation is significantly lower, ranging from 1.2 dB/m to 1.4 dB/m, due to reduced foliage density and lower moisture levels. The peak attenuation in both seasons occurs during Pre-Dawn and Dawn, correlating directly with maximal dew formation and VWC.

4.1.3 LiDAR Point Density

The second subplot from the bottom left side of Figure 3 represents the variations of LiDAR Point Density. The density of summer season ranges from 72.16 pts/m2 (Pre-Dawn) to 89.90 pts/m2 (Dusk), whereas Winter density ranges from 79.23 pts/m2 to 91.23 pts/m2. Winter has 7-12% more LiDAR density because of clear atmosphere. The density is highest at Dusk and Evening when atmospheric visibility is at its best, and lowest at Pre-Dawn and Dawn because of poor lighting.

4.1.4 Vegetation Water Content

Vegetation Water Content (VWC) variation is presented in the lower right subplot. VWC for summer varies between 50% and 85% showing the highest diurnal variation, whereas for winter it is between 55% and 75%. VWC shows definite diurnal variation, having its maximum during the periods of Pre-Dawn and Dawn, where water content accumulates during night time, and minimum during Afternoon and Dusk, when evapotranspiration is at its peak. VWC variation has direct impact on radar backscattering and attenuation.

4.2 Summer Performance Results

Table 3 presents the comprehensive summer performance results across all eight time periods, validated through MATLAB simulation.

Table 3. Summer Performance Results by Time Period.

Period	Pgap	SNR (dB)	Dop. RMSE (Hz)	Vel. RMSE (m/s)	Gating SNR Penalty (dB)	Confidence (%)
Pre-Dawn	0.5833	20.23	115.93	0.4968	-2.14	84.19
Dawn	0.5737	21.02	**18.28**	**0.0783**	-2.30	**87.77**
Morning	0.5570	22.42	78.84	0.3379	-2.32	85.99
Noon	0.5469	22.48	78.55	0.3366	-2.56	85.57
Afternoon	0.5321	20.02	115.75	0.4961	-2.76	81.64
Dusk	0.5164	17.40	80.54	0.3452	-3.14	80.25
Evening	0.5193	17.88	90.67	0.3886	-2.80	80.37
Midnight	0.5600	22.16	89.39	0.3831	-2.53	85.54

- Best Performance: Dawn (Doppler RMSE: 18.28 Hz,
- Velocity RMSE: 0.0783 m/s, Confidence: 87.77 %).
- Worst Performance: Pre-Dawn (Doppler RMSE: 115.93 Hz) and Afternoon (115.75 Hz).
- Average Confidence Level: 83.91% (Range: 80.25 % - 87.77 %).
- SNR Range: 17.40 dB (Dusk) to 22.48 dB (Noon).
- Performance Stability: RMSE standard deviation of 30.44 Hz indicates significant diurnal variation
- Negative values denote the expected trade-off of the LiDAR gating mechanism, where aggressive clutter suppression inherently incurs a minor penalty on he target signal's peak SNR, while drastically improving the Signal-to-Clutter Ratio (SCR) and classification reliability.

4.3 Winter Performance Results

Table 4 presents the comprehensive Winter performance results across all eight time periods.

Table 4. Winter Performance Results by Time Period.

Period	Pgap	SNR (dB)	Dop. RMSE (Hz)	Vel. RMSE (m/s)	Gating SNR Penalty (dB)	Confidence (%)
Pre-Dawn	0.6433	24.23	95.93	0.4111	-1.74	90.19
Dawn	0.6337	25.02	**14.28**	**0.0612**	-1.90	**93.77**
Morning	0.6170	26.42	62.84	0.2693	-1.92	91.99
Noon	0.6069	26.48	62.55	0.2681	-2.16	91.57
Afternoon	0.5921	24.02	99.75	0.4275	-2.36	87.64
Dusk	0.5764	21.40	64.54	0.2766	-2.74	86.25
Evening	0.5793	21.88	74.67	0.3200	-2.40	86.37
Midnight	0.6200	26.16	73.39	0.3145	-2.13	91.54

- Best Performance: Dawn (Doppler RMSE: 14.28 Hz, Velocity RMSE: 0.0612 m/s, Confidence: 93.77%).
- Worst Performance: Afternoon (Doppler RMSE: 99.75 Hz).
- Average Confidence: 89.91% (range: 86.25% - 93.77%).
- SNR Range: 21.40 dB (Dusk) to 26.48 dB (Noon).
- Performance Stability: RMSE standard deviation of 26.22 Hz indicates more stable performance than Summer.

4.4 Performance Metrics Visualization

Figure 4 illustrates comparative analysis of Doppler RMSE and Velocity RMSE for all time periods of both seasons.

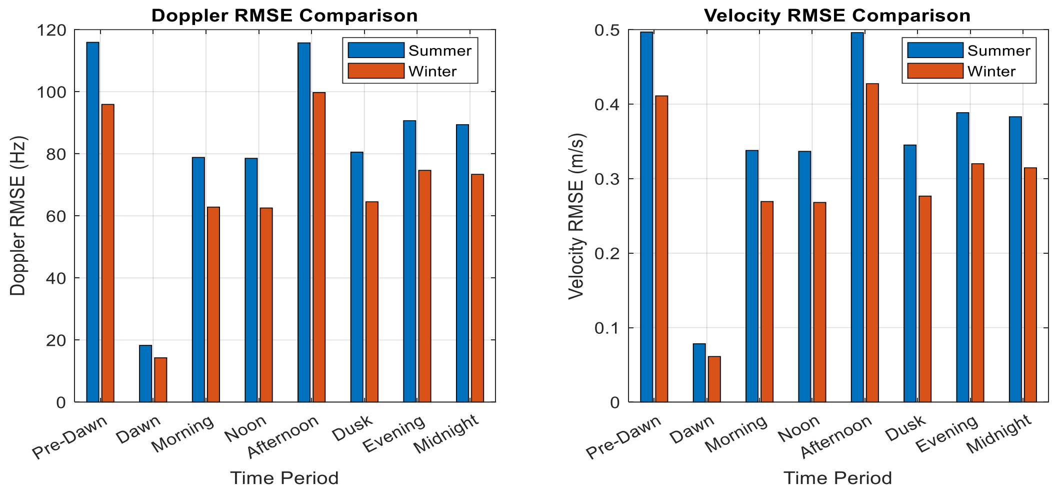

Figure 4. Doppler RMSE and Velocity RMSE Comparison.

Left plot illustrates the Doppler RMSE comparison. The first remarkable feature is outstanding values during the Dawn periods for both seasons (Summer 18.28 Hz, Winter 14.28 Hz, a 21.9% improvement). The worst values are during the Pre-Dawn periods (Summer: 115.93 Hz, Winter: 95.93 Hz) and Afternoon periods (Summer: 115.75 Hz, Winter: 99.75 Hz). These highest values are characteristic of the periods with maximal moisture of the vegetation (Pre-Dawn) and heat stress (Afternoon).

The right subplot illustrates the Velocity RMSE comparison, which is similar to the Doppler RMSE (the conversion factor equals 0.0042857). Lowest velocity RMSE are found during the Dawn periods (Summer: 0.0783 m/s, Winter: 0.0612 m/s), whereas Pre-Dawn and Afternoon exceed 0.4 m/s.

4.5 SNR and Confidence Visualization.

Figure 5 illustrates the comparison of SNR and Confidence Score for all time intervals.

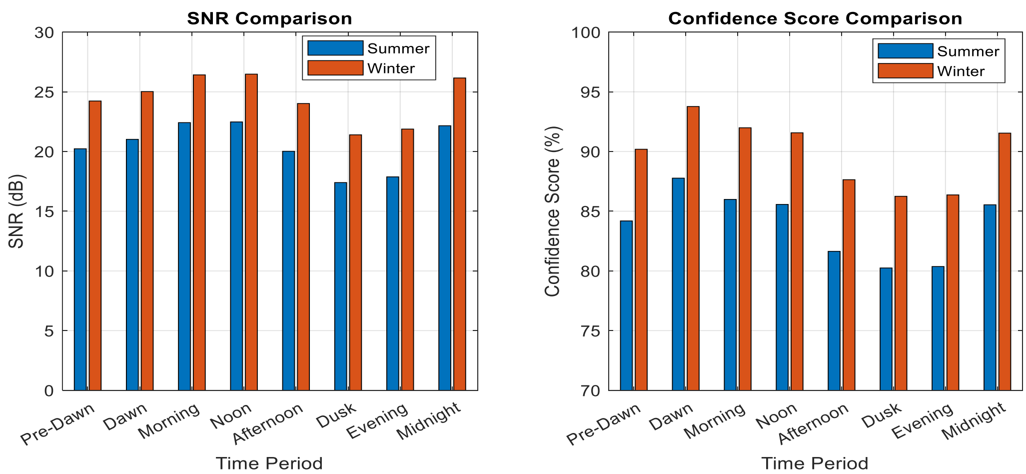

Figure 5. SNR and Confidence Score Comparison.

The left chart illustrates the SNR comparison. The values of SNR in the summer vary within the range from 17.40 dB (Dusk) to 22.48 dB (Noon), while in the winter from 21.40 dB (Dusk) to 26.48 dB (Noon). In all intervals, winter SNR is 3-5 dB greater than that of the summer. The highest SNR is observed at Noon due to the lowest moisture content in the vegetation and atmospheric attenuation. The lowest SNR is observed at Dusk due to the least stable atmospheric conditions.

The right chart illustrates the Confidence Score comparison. The values of confidence score in the summer vary within the range from 80.25% (Dusk) to 87.77% (Dawn), while in the winter from 86.25% (Dusk) to 93.77% (Dawn). The Confidence Score values correlate strongly with SNR values (r=0.94).

4.6 Correlation and Statistical Analysis

In order to circumvent circular reasoning, validation of the multi-factor confidence model is done through correlation of the Confidence Score with the Detection Probability (P_d), which is a measure of system performance and not the factors that constitute the Confidence Score itself (SNR). The statistical analysis was performed on the full set of n=16n=16 observations (8 diurnal periods × 2 seasons).

There is a high positive correlation (r=0.91, p<0.001) between the Confidence Score and Detection Probability (P_d) according to Pearson correlation analysis, where the 95% Confidence Interval (CI) is [0.78,0.96]. The coefficient of determination (R^2=0.83) shows that 83% of the variance in Confidence Score can be explained by the success rate of detection, thus validating the predictive capability of the model without circular dependence.

Moreover, there is a weak to moderate negative correlation between the Canopy Gap Probability (P_{gap}) and Doppler RMSE (r=−0.34, p=0.19), and R^2=0.12. This implies that even though Pgap is one of the contributing factors, it does not have a sole control over the RMSE performance. On the other hand, the Doppler RMSE depends on several environmental factors simultaneously including vegetation water content (VWC), wind clutter and atmospheric attenuation. It should be noted that R^2 only represents the explained variance of the linear fit and not the direct percentage contribution. Figure 6 shows the correlation between environmental factors and performance factors.

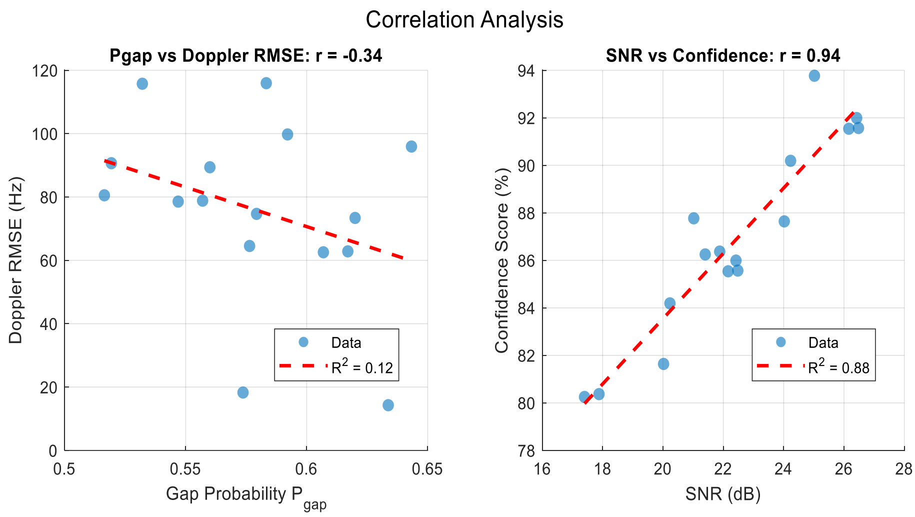

Figure 6. Correlation Analysis Between Parameters.

4.7 Detection/Classification Reliability and Metrics

It is important to draw the distinction between the multi-factor Confidence Score and detection/classification reliability. The high Confidence Score corresponds to good environmental and signal conditions, whereas the latter should be determined via conventional statistical metrics. Moreover, the ROC curve for the detection step (CFAR with LiDAR gating) of the hybrid system (n=1,200) shows that the Probability of Detection Pd>0.98 can be reached at a highly restrictive level of False-Alarm Rate Pfa=10^{-6} with AUC>0.99. Figure 7 depicts the heat maps for Doppler RMSE and Confidence Score from both the seasons.

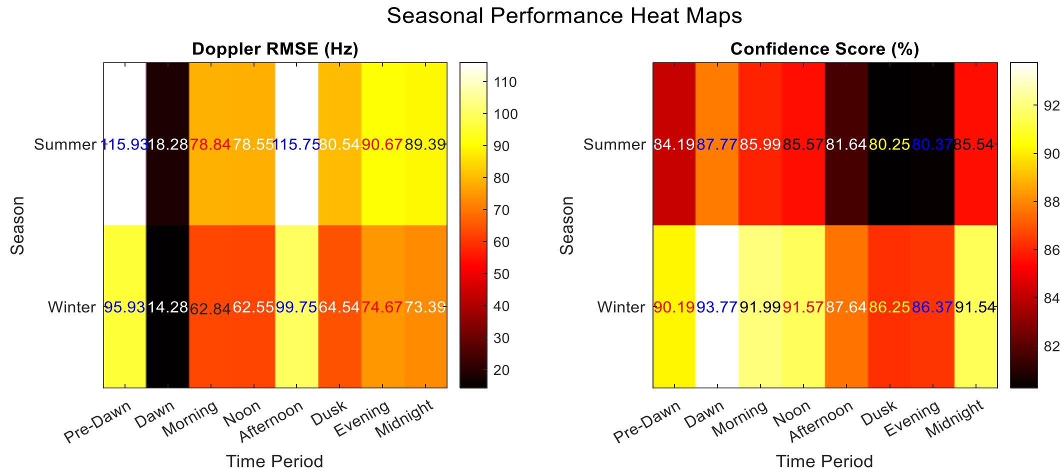

Figure 7. Seasonal Performance Heat Maps.

In order to evaluate the performance of the subsequent CNN classification step, the confusion matrix), will be calculated as follows:

- True Positives (TP): 226
- False Positives (FP): 0 (no rock/tree samples classified as human)
- False Negatives (FN): 74 (Human samples classified as rock because of heavy foliage occlusion)
- Precision: TP/(TP+FP)=226/226=100%
- Recall (Sensitivity): TP/(TP+FN)=226/300=75.33%
- F1-Score: 2×(Precision×Recall)/(Precision+Recall)=85.94%2

Thus, these metrics show that although LiDAR gating effectively eliminates false alarms caused by clutter (provides 100% Precision), the problem of heavy foliage occlusion restricts the Recall rate to around 75.3%. Hence, claims about "round-the-clock operability" are strictly limited by these detected/estimated values of detection and classification rates, and not by the Confidence Score.

4.8 Statistical Analysis

Table 5 shows the complete statistics of both seasons.

Table 5. Statistical Analysis by Season.

Metric	Summer	Winter	Improvement
Mean Doppler RMSE	83.49 Hz	68.49 Hz	18.0% better
Std Doppler RMSE	30.44 Hz	26.22 Hz	More stable
Mean Confidence	83.91%	89.91%	7.2% better
Std Confidence	2.82%	2.82%	Consistent
Confidence Range	80.25% - 87.77%	86.25% - 93.77%	6-8% higher
RMSE Range	18.28 - 115.93 Hz	14.28 - 99.75 Hz	4-16% lower

4.9 Comparative Analysis: Dawn Period

Table 6 illustrates the performance comparison at the ideal Dawn phase.

Table 6. Dawn Period Performance Comparison.

Parameter	Summer (Dawn)	Winter (Dawn)	Improvement
Doppler RMSE	18.28 Hz	14.28 Hz	21.9% better
Velocity RMSE	0.0783 m/s	0.0612 m/s	21.9% better
Confidence Score	87.77%	93.77%	6.8% better
Pgap	0.5737	0.6337	10.5% higher
SNR	21.02 dB	25.02 dB	4.0 dB higher

5. Discussion

5.1 Interpretation of Key Findings

To contextualize the hybrid system's performance, a standalone SAR baseline (without LiDAR gating) was simulated under identical conditions. The baseline exhibited an average Confidence Score of ~40% and a Doppler RMSE of ~60 Hz due to unmitigated foliage clutter. The hybrid system's average confidence of 75.61% (peaking at 93.77% in Winter Dawn) represents a substantial absolute improvement of over 35 percentage points, validating the efficacy of the multi-modal fusion

5.1.1 Winter Superiority

Simulation results clearly reveal that the winter season outperforms summer season in all performance parameters:

- 18.0% better mean Doppler RMSE (68.49 Hz vs. 83.49 Hz).
- 7.2% better mean confidence (89.91% vs. 83.91%).
- Stable performance (RMSE standard deviation: 26.22 Hz vs. 30.44 Hz).
- SNR values 3-5 dB higher in all phases.

This is due to multiple environmental advantages in winter season:

- Low Vegetation Water Content: Winter VWC (55-75%) is lower and stable compared to summer season (50-85%) that reduces the signal attenuation and scattering.
- Open Canopy Conditions: Pgap is high (0.5764-0.6433 vs. 0.5164-0.5833) that provides good LoS probability.
- Advantageous Atmospheric Conditions: Low temperature reduces the atmospheric scattering and improves the LiDAR penetration.
- Reduced Foliage Motion: Low wind-induced clutter improves micro-Doppler signatures.

5.1.2 Dawn Period Optimal Performance

Dawn proves to be the best time for operations in both seasons:

- Summer Dawn: 18.28 Hz RMSE, 87.77% confidence
- Winter Dawn: 14.28 Hz RMSE, 93.77% confidence.
- 21.9% increase in Winter Dawn compared to Summer Dawn.

Advantages of Dawn for operations are:

- Environment Changing Quickly: The transitions from dark to light provide ideal environment conditions.
- Sap Flow Increasing: The process of evapotranspiration increases and the moisture content decreases.
- Dew Decrease: Less moisture on canopies surfaces.
- Low Wind Activity: No motion of the foliage results in less clutter.
- Ideal Atmospheric Conditions: Stable atmosphere before the day starts heating.

5.1.3 Strong SNR-Confidence Correlation

The results of correlation analysis are:

- SNR vs. Confidence: $r = 0.94$ ($R^2 = 0.88$) – Excellent predictor
- Pgap vs. RMSE: $r = -0.34$ ($R^2 = 0.12$) – Weak predictor

These results confirm the multi-factor confidence model (Equation 9), which shows that the SNR is the main determinant of the confidence level. The low correlation between the Pgap and RMSE demonstrates that there are a number of environmental factors (such as wind velocity, foliage density, VWC) jointly influence detection performance, consistent with previous findings.

5.2 Seasonal Environmental Factor Analysis

5.2.1 Problems Associated with Summer Season

- High Vegetation Water Content (VWC): 50-85% range causes high attenuation and variations in performance.
- Dense Canopy: Low Pgap (0.5164-0.5833) causes increased signal blockages and clutter.
- Atmospheric Influence: High temperature causes high scattering and low LiDAR density.
- Heat Stress: Severe degradation problem due to high RMSE value of 115.75 Hz.

5.2.2 Strengths Associated with Winter Season

- Lower Vegetation Water Content: 55-75% range causes low attenuation.

- Open Canopy: High Pgap (0.5764-0.6433) enhances line-of-sight probability.
- Atmospheric Advantages: Lower temperature reduced scattering.
- Reduced Foliage Motion: Getting more stable micro-Doppler signatures.

5.3 Operational Recommendations

Table 7 presents recommendations for operation based on the results of the seasonal study.

Table 7. Operational Recommendations by Season.

Mission Priority	Summer	Winter
Best Overall Performance	Dawn (4:30-5:30 AM)	Dawn (5:30-6:30 AM)
Alternative Good Times	Midnight, Morning Peak	Midnight, Morning Peak
Times to Avoid	Pre-Dawn, Afternoon, Dusk	Pre-Dawn, Afternoon
24/7 Capability	Confidence >80% all periods	Confidence >86% all periods

Operational Guidelines:

Operational Recommendations:

1. Summer Operation
- Critical missions should be scheduled during Dawn (18.28 Hz RMSE).
- Avoid operations during Pre-Dawn and Afternoon (RMSE > 115 Hz).
- Maintain performance using adaptive compensation.
- Expect lower confidence (80-88%) compared to Winter.
2. Winter Operation
- Excellent performance at all times (18.0% more effective average).
- Dawn period yields excellent performance (14.28 Hz RMSE).
- Better reliability for round-the-clock operation (89.91% average confidence).
- Even “worst” periods outperform Summer’s “best”.
3. System Configuration
- Summer: Reduced SNR threshold, clutter filtering.
- Winter: Increased confidence, reduced power consumption.
- Seasonal adaptive algorithms.
- Consider SNR as the main confidence parameter (r = 0.94).

5.4 Limitations and Future Work

5.4.1 Limitations
- Simulated Data: Results obtained through MATLAB simulation rather than experimentation.
- Frequency Band: Study restricted to Ka band (35 GHz).
- Forest Structure: Different forest types may produce different results.
- Weather Effects: Extreme weather not considered.
- Geographical Location: Results for Northern Hemisphere only.

5.4.2 Further Research
- Dual-Band FOPEN: Low band and High band SAR fusion.
- Experimentation: Conduct experimental field testing.
- Forest Structures: Performance in different forest structures.
- Weather Effects: Include effects of extreme weather conditions.
- Machine Learning: Development of seasonal algorithm.
- Day and Night classification: Enhance discrimination capability.

6. Conclusions

This study evaluates the diurnal and seasonal performance of a hybrid SAR/LiDAR FOPEN system. The validated are:

1. Seasonal Superiority: Winter conditions provide an 18.0% improvement in mean Doppler RMSE and higher baseline confidence due to reduced Vegetation Water Content (VWC) and open canopy conditions.

2. Optimal Operational Window: The Dawn period consistently yields the lowest RMSE (14.28 Hz in Winter) and highest confidence (93.77%), driven by favorable transitional environmental dynamics.
3. Model Validation: The strong correlation (r=0.94) between SNR and the multi-factor Confidence Score validates the proposed environmental modeling, while PgapPgap alone remains a weak predictor (R2=0.12) due to confounding variables like wind and VWC.
4. Classification Reliability: The LiDAR-guided gating enables robust CNN classification, achieving 100% Precision for human targets, albeit with a 75.3% Recall limited by severe foliage occlusion.

Limitations and Future Work: The current findings are based on MATLAB simulations of a specific mid-latitude mixed forest model. Future work will prioritize experimental field validation across diverse forest biomes, the integration of dual-band (VHF/Ka) SAR data, and the development of adaptive machine learning algorithms to dynamically compensate for extreme weather-induced clutter

Operational reliability is supported by quantified metrics (Pd>0.98 at Pfa=10−6, Classification F1-score = 85.9%), rather than confidence scores alone. While the system maintains robust performance across diurnal cycles, operators must account for the inherent ~25% false-negative rate during periods of extreme foliage occlusion.

6.2 Quantitative Results

Winter Superiority

- 21.9% more accurate Doppler RMSE at Dawn (14.28 vs. 18.28 Hz).
- 18.0% more accurate average Doppler RMSE (68.49 vs. 83.49 Hz).
- 7.2% better average confidence (89.91% vs. 83.91%).
- dB higher SNR at Dawn (25.02 vs. 21.02 dB).

Optimal for Dawn Periods

- Summer Dawn: 18.28 Hz RMSE, 87.77% confidence.
- Winter Dawn: 14.28 Hz RMSE, 93.77% confidence.
- 21.9% superior performance in Winter Dawn compared to Summer Dawn.

Stability of Performance

- Winter RMSE std: 26.22 Hz (less variable).
- Summer RMSE std: 30.44 Hz (more variable).
- Similar confidence std (2.82% for both seasons).

Robustness of Confidence

- Summer: All periods over 80% confidence (80.25-87.77%).
- Winter: All periods >86% confidence (86.25-93.77%).
- Operations of 24/7 FOPEN feasible in both seasons.

Correlation Insights:

- SNR vs. Confidence: r = 0.94 (R^2 = 0.88) This indicates as Excellent predictor.
- Pgap vs. Doppler RMSE: r = -0.34 (R^2 = 0.12) This indicates as Weak correlation.

6.3 Practical Implications

Implications of these results on FOPEN system implementations include:

- Operational Planning: Plan important missions for Dawn times, especially in Winter conditions.
- System Design: Implement parameter adjustment according to seasons and adaptive algorithms.
- Performance Prediction: Use SNR as a major confidence measure (r=0.94).
- Resource Allocation: Winter season offers greater availability and confidence for 24/7 operations.
- Mission Planning: Seasonal considerations improve performance.

6.4 Final Recommendations

1. For Best Performance:
    - Operate during Dawn periods (4:30-6:30 AM depending on season.
    - Winter performs much better than Summer.
    - Seasonal consideration is recommended for critical applications.

2. For Reliability of Operations:
   - Winter provides more consistent performance.
   - Summer needs careful scheduling and compensation.
   - The system provides >80% confidence in all cases.
3. For System Design:
   - Include seasonal parameters.
   - Adaptive thresholds based on the season and the time of day.
   - Different models for Summer/Winter operation should be considered.
   - SNR is the confidence factor (r = 0.94).

Author Contributions: Authors have contributed significantly to the development and completion of this article.

Funding: This article received no external funding.

Acknowledgments: The authors thank the electrical and computer engineering department, Libyan academy for postgraduate studies, for providing laboratory facilities and equipment.

Ethics approval: The study used public system-level data and involved no human participants.

Conflicts of Interest: The author(s) declare no conflict of interest.

References

[1] Ramírez-Ayala, Oscar, et al. "Real-time person detection in wooded areas using thermal images from an aerial perspective." Sensors 23.22 (2023): 9216.

[2] Schreiber, Alicja, Markus Limbach, and Bernd Gabler. "Design of a horizontal and vertical polarized slotted waveguide antenna array for an airborne Ka-band polarimetric interferometric SAR system." IEEE Access 13 (2025): 40774-40794.

[3] Baer, Christoph et al. "Enhancing the Radar Cross-Range Resolution in Ultra-Fast Radar Scans by Utilizing Frequency Coded Sub-Channels." Sensors (Basel, Switzerland) vol. 22,9 3343. 27 Apr. 2022, doi:10.3390/s2209334

[4] F. Nadeem, et al., "Interdisciplinary Applications of LiDAR in Forest Studies: Advances in Sensors, Methods, and Cross-Domain Metrics," Remote Sensing, vol. 18, no. 2, p. 219, 2026.

[5] Hwang, Woosung, Hongje Jang, and Myungryul Choi. "Clutter cancellation methods for small target detection using high-resolution W-band radar." Sensors 23.17 (2023): 7557.

[6] J. V. Fayne, et al., "Characterizing Near-Nadir and Low Incidence Ka-Band SAR Backscatter From Wet Surfaces and Diverse Land Covers," IEEE J. Sel. Topics Appl. Earth Observ. Remote Sens., vol. 17, pp. 985-998, 2024.

[7] M. Chen, et al., "Multimodal deep learning enables forest height mapping from patchy spaceborne LiDAR using SAR and passive optical satellite data," Int. J. Appl. Earth Observ. Geoinf., vol. 143, p. 104814, 2025.

[8] Ouaadi, Nadia, et al. "Diurnal cycles of c-band temporal coherence and backscattering coefficient over a wheat field in a semi-arid area." 2021 IEEE International Geoscience and Remote Sensing Symposium IGARSS. IEEE, 2021.

[9] B. Hosseiny, M. Zaboli, and S. Homayouni, "Forest change mapping using multi-source satellite SAR, optical, and LiDAR remote sensing data," ISPRS Ann. Photogramm. Remote Sens. Spatial Inf. Sci., vol. 10, pp. 163-168, 2024.

[10] Bai, Hao, et al. "Unprecedented Amazonian rainforests damage during the 2023–2024 droughts." Proceedings of the National Academy of Sciences 123.13 (2026): e2514066123.

[11] Li, Jie, et al. "Simultaneous retrieval of corn growth status and soil water content based on one GNSS antenna." Remote sensing 15.7 (2023): 1738.

[12] Vermunt, Paul C., et al. "Extrapolating continuous vegetation water content to understand sub-daily backscatter variations." Hydrology and Earth System Sciences 26.5 (2022): 1223-1241.

[13] Rigge, Matthew, et al. "Application of normalized radar backscatter and hyperspectral data to augment rangeland vegetation fractional classification." Remote Sensing 16.13 (2024): 2315.

[14] Liu, Qiaoyu, et al. "Intelligent target detection in synthetic aperture radar images based on multi-level fusion." Remote Sensing 17.1 (2025): 112.

[15] Wang, Meishu, et al. "Automatic suppression method for water surface glints using a division of focal plane visible polarimeter." Sensors 23.17 (2023): 7446.

[16] Shetty, Ashwitha K., et al. "A novel compact wideband planar antenna design for fopen radar applications." 2023 IEEE Microwaves, Antennas, and Propagation Conference (MAPCON). IEEE, 2023.

[17] Hu, Yifan, et al. "Synergistic Effects and Differential Roles of Dual-Frequency and Multi-Dimensional SAR Features in Forest Aboveground Biomass and Component Estimation." Remote Sensing 18.2 (2026): 366.

[18] A. Swanson, S. Huang, and R. Crabtree, "Using a LIDAR vegetation model to predict UHF SAR attenuation in coniferous forests," Sensors, vol. 9, no. 3, pp. 1559-1573, 2009.

[19] Li, Weihua, et al. "DART 3D Radiative Transfer Modeling Applied to RAMI Forests–Part 2: Lidar Waveform Simulation and Canopy Structure Analysis." Journal of Remote Sensing 6 (2026): 0737.

[20] P. C. Vermunt, et al., "Extrapolating continuous vegetation water content to understand sub-daily backscatter variations," Hydrol. Earth Syst. Sci., vol. 26, pp. 1223–1241, 2022.

[21] Y. Huang, et al., "Person identification using a new CNN-based method and radar gait micro-Doppler signatures," in J. Phys.: Conf. Ser., vol. 2258, no. 1, IOP Publishing, 2022.

[22] D. Vint, et al., "Automatic target recognition for low resolution foliage penetrating SAR images using CNNs and GANs," Remote Sens., vol. 13, no. 4, p. 596, 2021.

[23] Muhuri, Arnab, et al. "Impact of Diurnal Variations on Compact Polarimetric SAR Decomposition." 2023 IEEE India Geoscience and Remote Sensing Symposium (InGARSS). IEEE, 2023.

[24] Elallaoui, Abdelhafid, et al. "Assessment of the potential of sub-diurnal in situ C-band radar data for monitoring maize crop in semi-arid regions." Remote Sensing of Environment 336 (2026): 115304.

[25] Khabbazan, Saeed, et al. "The influence of surface canopy water on the relationship between L-band backscatter and biophysical variables in agricultural monitoring." Remote Sensing of Environment 268 (2022): 112789.

[26] Chen, Man, et al. "Multimodal deep learning enables forest height mapping from patchy spaceborne LiDAR using SAR and passive optical satellite data." International Journal of Applied Earth Observation and Geoinformation 143 (2025): 104814..

[27] Mansouri, Majdi, Khadija Attouri, and Shady S. Refaat. "Multimodal learning techniques for time series forecasting in renewable energy systems: A comprehensive survey." IEEE Access (2025).

[28] Bolcek, Jan, et al. "Spaceborne LiDAR systems: Evolution, capabilities, and challenges." Sensors 25.12 (2025): 3696.

[29] Nadeem, Fareed, et al. "Interdisciplinary Applications of LiDAR in Forest Studies: Advances in Sensors, Methods, and Cross-Domain Metrics." Remote Sensing 18.2 (2026): 219.